# Simulations of the Absorption and Fluorescence of Indole in Aqueous Solution and at a Nonpolar/Polar Interface

**Anders Öhrn* and Gunnar Karlström**

*Department of Theoretical Chemistry, Chemical Center, P.O. Box 124, S-221 00 Lund, Sweden*

*Received: June 8, 2007; In Final Form: July 25, 2007*

Theoretical results are presented on the absorption and fluorescence of indole in aqueous solution as well as at the air/water surface. We use a combined quantum chemical statistical mechanical model with explicit solvent. An approximate ab initio complete active space self-consistent field description of the indole molecule is used, coupled to a discrete polarizable water medium. From the bulk simulations, strong support is found for the interchange mechanism, which explains the unusual solvent shift of the fluorescence of indole or tryptophan in a polar surrounding by a solvent induced switch of the fluorescing state. Two mechanisms are given to explain the different shifts for indole at the interface. First, a dielectric depletion effect, which is expected from the reduction of the amount of polar media. Second, an interface-specific effect, which derives from the stronger hydrogen bond formation at the surface. The latter effect acts to increase the shift for both absorption and emission at the surface as compared to the bulk. From these results, the intrinsic probe photophysics of tryptophan in proteins is discussed in terms of the properties of the protein/solvent interface and the orientation of the amino acid.

## 1. Introduction

In 1876 the term "chromophore" was coined by Witt to describe the connection between chemical structure and the ability of a substance to give color.[1] The basic research on chemical structure and optical properties, which Witt's work was part of, was, according to some historians, the foundation for the successful German chemical industry that developed during the following decades.[2−4] The understanding of chromophores has improved greatly since the late nineteenth century, and the fundamental connection between electronic structure (and as a consequence chemical structure) and optical properties is nowadays well studied, not least by quantum chemical methods. From the connection between electronic structure and optical properties, it follows that the latter properties will change when the electronic structure changes in response to a perturbation of some sort from the environment of the chromophore. The halochromism of pH-indicators, the empirical parameters of solvent polarity from spectroscopic measurements, and the suggestion by Kasha to differentiate $n \rightarrow \pi^*$ transitions from $\pi \rightarrow \pi^*$ transitions by monitoring the sensitivity of the respective peaks to different solvents are but three examples where the above mechanism operates.[5−8] A more recent and quite popular technique based on the same mechanism is the use of fluorescing molecular probes to study protein structure and folding.[9−12] The basic idea to some of these fluorescence techniques is that changes in the protein structure lead to different environments of the chromophore, often interpreted in terms of more or less exposure of the probe to the aqueous surrounding. A variety of external probes have been synthesized to be attached to a protein to monitor different perturbations. Intrinsic probes exist as well, which are amino acids with polarity-sensitive fluorescence spectra.

Tryptophan is the most common amino acid used as an intrinsic probe of local polarity in proteins. Its chromophore is indole, which has the structure of benzene fused with pyrrole. It is well-known that the fluorescence, in contrast to the absorption, of indole is very sensitive to the solvent polarity.[13−19] The two lowest excited states of indole (and tryptophan), which are thought to be the relevant states in the intrinsic probe mechanism, are called $L_a$ and $L_b$ in analogy with Platt's nomenclature for systems such as benzene and naphthalene.[20,21] The cause of the peculiar solvent dependence of indole and tryptophan has been debated. Either some form of excited solute−solvent complex or an $L_a$−$L_b$ state interchange, induced by usual electrostatic interactions, have been given as explanations.[16,22−25] Nowadays, the consensus is that the $L_a$−$L_b$ interchange mechanism is the best available one, based on both recent experiments that fail to confirm the existence of a water−excited indole complex and theoretical calculations that, one way or another, support the hypothesis of an interchange from ordinary solute−solvent interactions. The interchange mechanism implies, according to Kasha's rule, that when the $L_a$ state becomes lower in energy than the $L_b$ state in a polar environment, the $L_a$ state will be the fluorescing state, in contrast to the situation in a nonpolar environment.[5] The reason the interchange can be induced by the polar environment is that the $L_a$ state has a greater polarity and polarizability than the $L_b$ state.[23,26−33]

In the present study, we run Monte Carlo simulations of indole in aqueous solution to study its absorption and fluorescence spectra. The model combines ab initio quantum chemistry with a classical force-field for the water molecules. No experimental data is used as input into the model; therefore, our results cannot be biased to reproduce certain results or skewed by false interpretation of experiments. This gives confidence to the microscopic molecular interpretations to the observed experimental results, given, of course, that the latter ones are reproduced with adequate accuracy by the model. As will be seen, our results give strong support to the $L_a$−$L_b$

* To whom correspondence should be addressed. E-mail: anders.ohrn@teokem.lu.se.

10.1021/jp0744477 CCC: $37.00 
Published on Web 10/03/2007

interchange mechanism. A protein environment to a chromophore is, in contrast to the aqueous bulk, heterogeneous on account of the constraints put on the orientation of the chromophore by the covalent bonds to the peptide chain. This means, on the one hand, that the solvent can be more or less excluded from certain volumes around the indole chromophore and, on the other hand, that charged or dipolar groups of the remaining protein can perturb the electronic structure of the chromophore and, thus, the spectrum.[29,34−36] To accurately model the photophysics in a protein is a very challenging task. Although protein simulations are improving, experimental input and notable simplifications of the model, on account of the size and complexity of the system, are both needed. There is a risk that biases and uncertainties are introduced into the model. Vivian and Callis, as well as Rogers et al., have modeled tryptophan in proteins with some success,[29,37] but Rogers et al. conclude that it is clear from their studies "that even small changes of the atomistic environment may lead to significant changes of the transition energies of the indole excited states" and that this sheds light on the challenges of atomistic simulations.[37] In the present study we take a different approach to investigating the properties of tryptophan in a protein environment. Instead of trying to model the actual proteins, we study a different heterogeneous environment, namely, the air/water interface. It is possible to model this surrounding with the same accuracy and confidence as the bulk solvation with the present model; hence, the results thus obtained are free from the uncertainty that experimental input and major model simplifications bring. From a careful analysis of this system and its relation to the bulk simulations, a number of principles are theoretically established. These principles are then used to discuss the situation in a protein environment. Clearly, this approach is incomplete because we do not study the actual protein from first principles. However, we believe that the incompleteness of our "model path" is more transparent than in the path going over a not entirely reliable protein simulation, and thus our study will provide further insight into the photophysics of tryptophan in proteins. We note that studies of optical properties of molecules adsorbed at surfaces and interfaces are themselves of interest.[38−43]

The study of the excited-state of indole has recently come to focus on the $\pi\sigma^*$ state that lies above $L_a$ and $L_b$. Although we have not studied this state, we should provide a few comments on the relevance of this state for the fluorescence of indole in a polar surrounding. From quantum chemical calculations, Sobolewski and Domcke predict that the diffuse and dipolar $\pi\sigma^*$ state is dissociative, with the N−H bond being broken.[44] Recent experiments find support for the existence of this nonradiative process in indole.[45,46] Dedonder-Lardeux et al. theoretically show that large electric fields in certain directions on indole can not only switch the order of the $L_a$ and $L_b$ states but that they also make the $\pi\sigma^*$ the lowest state.[47] This effect is a result of the significant polarity of the $\pi\sigma^*$ state. From simulations of the indole−water system, Dedonder-Lardeux et al. find that the electric perturbation from the solvent is quite large and conclude that the $\pi\sigma^*$ state will be close enough to the $L_a$ and $L_b$ states for mixing to occur in some solvent configurations. However, because the $\pi\sigma^*$ state is not only polar but also is very diffuse with a significant Rydberg character (Serrano-Andrés and Roos prefer to identify the state as a 3s-Rydberg state), there will also be a repulsive perturbation from the solvent because of the antisymmetry restrictions on the electrons.[27] In the terminology of Bayliss and McRae, this is the packing strain, which will raise the energy for the occupation of a diffuse state in a molecular environment.[48] Therefore, to quantify the degree to which the solvent perturbs the $\pi\sigma^*$ state relative to the $L_a$ and $L_b$ states, some account of the packing strain may be needed, and when taken into account, it is most likely to lead to an increase of the energy separation. From this we conclude that, in the complete perturbation from the aqueous environment, the radiative states $L_a$ and $L_b$ likely remain sufficiently separated from, and thus unperturbed by, the $\pi\sigma^*$ state for our simulations to be sound models of the intrinsic probe mechanism of indole without explicit inclusion of the $\pi\sigma^*$ state.

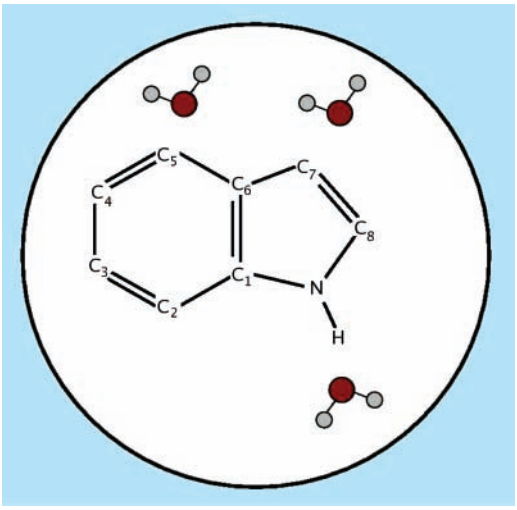


**Figure 1.** Schematic of the indole−water system in QMSTAT. Outside the spherical cavity is a dielectric continuum, with either permittivity $\epsilon = 80$ for the bulk simulations or $\epsilon = 1$ for the air/water interface simulations. The dimensions are distorted.

Below, we continue with a presentation of the model. Already published details are not recounted; we limit ourselves to key aspects and equations, as well as the specifics, for the indole system. After that, the results of the simulations are presented, first from the simulations of absorption and fluorescence in aqueous bulk, then from the interface simulations. The results are discussed, and the conclusions are summarized last.

## 2. Method and Simulation Protocol

The model we use is a combined quantum chemical statistical mechanical model, called QMSTAT, which uses a multiconfigurational ab initio description of the solute.[49,50] The solvent is represented as 150 explicit water molecules, with a simplified polarizable force-field description.[51] Four point-charges and three distributed polarizabilities are used for each water molecule, a distributed $1/r^6$ expression is used for the water−water dispersion interaction, and a distributed exponential expression, together with a term proportional to $1/r^{20}$ for very short-range separation, is used for the water−water exchange repulsion. To account for long-range effects, the molecular system is contained in a spherical dielectric cavity described within the image-charge approximation.[52,53] The boundary is impenetrable (so the number of molecules is the same during the simulation), and the radius is variable (so the pressure (1 atm) is the same during the simulation). In simulations of the air/water interface the dielectric continuum is removed, and a roughly spherical droplet of 150 water molecules and one indole molecule is formed. In Figure 1 the indole−water system is schematically represented, and the numbering of the carbon atoms is introduced.

Once the energy functional is defined (vide infra), the statistical mechanical problem is solved at constant temperature

($T = 300$ K) with the Metropolis−Monte Carlo algorithm.[54] Extensive sampling of the configurational space is done, and all simulations consist of $2.4 \times 10^6$ steps each, where all particles are moved in each step. Because we use a so-called hybrid approach to solve the statistical mechanical problem, which only contains a statistical error that tends to zero as the number of sampled points tends to infinity, the accuracy of the solution to the statistical mechanical part of the problem is high. See previous publications for more discussion of this aspect of QMSTAT, especially ref 55.

QMSTAT uses an effective quantum chemical representation of the solute, that is, the electronic Hamiltonian is written as shown in eq 1,

$$\hat{H}_{\text{eff}}(\vec{R}_{\text{solv}}) = \hat{H}_0 + \hat{V}_{\text{solv}}(\vec{R}_{\text{solv}}) \tag{1}$$

where $\hat{H}_0$ is the Hamiltonian for indole in the gas-phase, and $\hat{V}_{\text{solv}}$ is an approximate perturbation from the solvent, which depends on the solvent coordinates $\vec{R}_{\text{solv}}$. The $\hat{H}_{\text{eff}}$ term defines a Schrödinger equation, which can be approximately solved by some quantum chemical method. Originally, QMSTAT was formulated for the Hartree−Fock method.[56] A more recent extension uses a multiconfigurational method, which can describe states other than the ground state.[49,50] In this extension, the wave function for the solvated molecule is expanded in terms of a number of state wave functions (eq 2),

$$\Psi_i^{\text{eff}} = \sum_j c_{ij}\Psi_j \tag{2}$$

where $\Psi_i^{\text{eff}}$ is the eigenfunction to the $i$th eigenvalue to the effective Schrödinger equation, $\{\Psi_j\}_j$ is a set of basis states, and $c_{ij}$ are variationally determined constants. The following procedure is used to obtain a state basis for a given geometry of indole; the complete active space self-consistent field (CASSCF) method is used to obtain states for the indole ground state ($S_0$) and the excited states $L_b$ and $L_a$ for the Hamiltonian $\hat{H}_0$.[57−59] The active space consists of the four $\pi$-orbitals, the four $\pi$*-orbitals, and the nonbonded orbital on the nitrogen atom. This is the active space recommended by Serrano-Andrés and Roos in their calculation of the gas-phase spectrum of indole.[27] The atomic natural orbital (ANO) basis set of Pierloot et al. is used with the contractions C,N/4s3p2d and H/3s2p.[60] The optimal gas-phase geometries for the respective states, obtained from optimizations with analytical gradients with the above basis set and active space, are used in the simulations.[61] The geometries are almost identical to the ones obtained and reported in ref 27. We do not optimize the geometries with the solvent present. This is an approximation because an environment can induce geometry changes, which in turn can change the energy difference of the relevant states. A full optimization of indole with the present model is not feasible, because it would involve the evaluation of a large number of numerical free-energy gradients. We do not expect large geometry changes given the large degree of conjugation (and hence rigidity), but we cannot completely rule out contributions from solvent-induced geometry changes. If the frozen gas-phase geometry assumption is highly invalid, this should clearly be seen in the comparison of the simulation result and experiment. As will be seen, the results below do not invalidate the frozen gas-phase geometry assumption, but still, some errors are expected from this assumption.

If only the three states above are included in the basis, then the polarizability of indole would be underestimated. Additional CASSCF states are therefore obtained to treat polarization. First, eighteen states are obtained by running calculations on the three states with homogeneous electric fields (magnitude 0.003 a.u.) along either the *x*-, *y*- or *z*-axis, one at a time and in both directions. Second, a set of inhomogeneous fields are constructed by (i) adding an ideal dipole of magnitude 1.27 D at 2.12 Å from the hydrogen atom bonded to the nitrogen atom, with a direction of the dipole such that it points at the hydrogen atom and forms a 45° angle with the N−H bond; four such calculations are done (the two possible with the dipole in the molecular plane, and the two with the dipole as far away from the plane as possible; see ref 50 for details, where a similar construction was used for *para*-benzoquinone). (ii) Ideal dipoles are also placed above the molecular plane with directions parallel to the normal vector to that plane; they are placed either 3.18 Å above or below the center of mass to the pyrrole part of indole or 3.18 Å above or below the center of mass to the benzene part; their magnitudes are 1.27 D. In total, 45 CASSCF states are produced for each of the three different geometries of indole. The states span a space capable of describing the $S_0$, $L_a$, and $L_b$ states of indole in the relevant geometry, either unperturbed, perturbed by a homogeneous electric field, perturbed by a selection of inhomogeneous electric fields, or any possible linear combination of these perturbations. It is shown in ref 50 that this type of construction leads to an excellent reproduction of the electric response properties of the CASSCF calculation in the full atomic basis set. The CASSCF states in this set are nonorthogonal. Hence, some complications in the implementation would occur if they were used as the basis in eq 2. We use the CAS state interaction (CASSI) method to obtain a set of orthogonal eigenstates to $\hat{H}_0$ that span the same space as the CASSCF states.[62,63] To improve efficiency, the contraction scheme described in ref 50 is used with threshold $t_d = 10^{-6}$. The three states from CASSI that are lowest in energy correspond to the unperturbed $S_0$, $L_b$, and $L_a$ states from CASSCF (in that order).

Because the relative energy difference between the states is fundamental to our study, we need to address the limitation of the CASSCF method in this respect. CASSCF generates good densities, but because of its incomplete account of the dynamic correlation, it usually fails to achieve quantitative accuracy for the energies. The CAS second-order perturbation (CASPT2) method is the preferred method to remedy this; the accuracy of CASPT2 is usually on the order 0.1 eV.[64−67] Parac and Grimme show that both time-dependent density functional theory and low-order coupled cluster calculations fail to describe the spectrum of indole (and similar molecules) with the same accuracy as a perturbation corrected multiconfigurational method.[68] We level-shift the three lowest CASSI states to the same relative energies as found with CASPT2 by Serrano-Andrés and Roos.[27] Observe that this does not modify the densities, only the relative energies and, to a minor extent, the polarizability. This way we get the best possible theoretical estimate of the original energy separation between $L_a$ and $L_b$; it also means that the limitations of the CASPT2 energies are inherited by our study.

The details of the formulation of $\hat{V}_{\text{solv}}$ are not repeated here. Suffice to say that it includes the important electrostatic interaction and also a pseudopotential-like operator to model the packing strain, which was mentioned in the Introduction. This operator is given in eq 3,

$$V_{\text{nel}} = d\sum_{k\in\Omega}\sum_l \epsilon_l |\chi_l^k\rangle\langle\chi_l^k| \tag{3}$$

where $d$ is a parameter, $\Omega$ is a subset of the explicit water molecules, $\chi_l^k$ is the $l$th occupied orbital of the $k$th solvent

**TABLE 1: Parameters for the Indole−Water Potential in QMSTAT[a]**

| interaction | parameter | value |
|---|---|---|
| repulsion | $d$ | −0.27 |
| | $\beta_4$ | 5.50 |
| | $\Omega$ | 10 |
| dispersion | $D_{C_1,O}$ and $D_{C_6,O}$ | 17.5 |
| | $DC_{1,H}$ and $D_{C_6,H}$ | 6.0 |
| | $D_{C}$non−shared,$_O$ | 23.2 |
| | $D_{C}$non−shared,$_H$ | 7.8 |
| | $D_{N,O}$ | 18.3 |
| | $D_{N,H}$ | 6.2 |
| | $D_{H,O}$ | 9.0 |
| | $D_{H,H}$ | 3.0 |

[a] For simulations of both absorption and fluorescence, the same values of the parameters are used. Observe that two different dispersion coefficients for the carbon atoms are used; see Figure 1 for notation. All parameters are in atomic units

molecule, and $\epsilon_l$ is the $l$th occupied orbital energy, which is the same for all water molecules because the solvent orbitals are frozen. The parameter to this operator is obtained in the same way as in previous studies, that is, the QMSTAT potential is fitted to the counterpoise corrected CASSCF supermolecular pair-potential.[69] At very short-range, the repulsion from $V_{\text{nel}}$, which scales as the solute−solvent overlap raised to the power of two ($S^2$), is not sufficient. Higher order terms are required but are only added as a contribution to the total energy, not as an operator. This contribution is defined by eq 4,

$$E_{S^4} = \beta_4 \left(\sum_{k\in\Omega}\sum_{l} \langle \Psi_i^{\text{eff}}|\chi_l^k\rangle \langle \chi_l^k|\Psi_i^{\text{eff}}\rangle\right)^2 \tag{4}$$

where $\beta_4$ is a parameter, and $\Psi_i^{\text{eff}}$ is the effective wave function for the solute. The parts of the potential included in the fit are (i) the hydrogen bonding between the oxygen atom on water and the hydrogen atom bonded to the nitrogen atom (this is known to be the strongest interaction between water and indole.[70,71]), and (ii) the weak bonding of water to the pyrrole part of indole.[72] Very good agreement is found between the QMSTAT pair-potential and the CASSCF reference.

The dispersion interaction between solute and solvent is not included in $\hat{V}_{\text{solv}}$ but is added phenomenologically as a distributed $1/r^6$ expression damped at short separations following Tang and Toennies (eq 5),

$$E_{\text{disp}} = -\sum_{k,l} \frac{D_{k,l}}{r_{kl}^{\,6}} f_{kl}(r_{kl}) \tag{5}$$

where $D_{k,l}$ are parameters, $k$ and $l$ are indices for atoms on solute and solvent, respectively, $r_{kl}$ is the atom−atom separation, and $f_{kl}$ is the damping function.[73,74] To make the distribution, we use a variant of the method by Becke and Johnson.[75,76] Becke and Johnson show that the molecular dispersion coefficient can be obtained fairly well by a simple relation that involves the static polarizability and the exchange-hole dipole moment (eq 6),

$$\langle d_X^2\rangle = \int \rho(r_1) d_X^2(r_1)\, \mathrm{d}r_1 \tag{6}$$

where

$$d_X^2(r_1) = \left(\frac{1}{\rho(r_1)} \sum_{ab} [\langle \psi_a|r|\psi_b\rangle \psi_a\psi_b(r_1)] - r_1\right)^2 \tag{7}$$

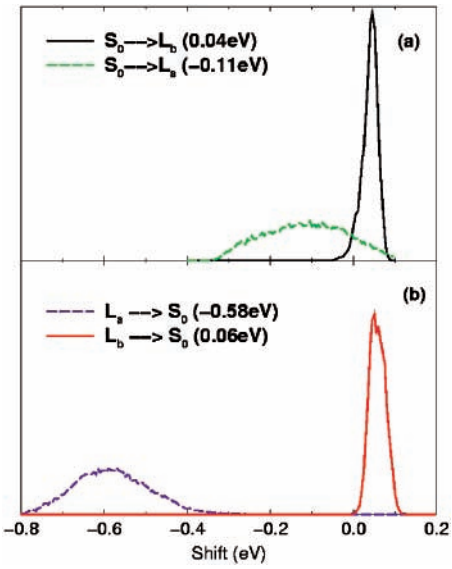


**Figure 2.** Solvent shift distributions for (a) the vertical absorption in indole in aqueous solution and (b) the vertical emission for the optimal geometry of the $L_a$ state in aqueous solution.

where $\rho$ is the electron density, and $\psi_a$ is an occupied HF molecular orbital. We use the quadrature of Lindh et al. to numerically evaluate the integral.[77] To distribute the dispersion coefficient over a number of atoms, we use the Loprop method, unlike Becke and Johnson who use a Hirschfeld partitioning.[78] Loprop constructs a localized basis in which the density in eq 6 is expanded. Individual terms are thus assigned to specific centers of indole, and together with the distributed polarizabilities given by Loprop, the Becke−Johnson (BJ) formula can be used to obtain the distributed coefficients. The magnitudes of the coefficients are, however, only defined ad hoc by the BJ formula. To get better absolute values for this study, we compute the full intermolecular second-order perturbation for the potentials described above as a reference, then the distributed coefficients are scaled uniformly to reproduce the dispersion reference curve. The relative values of the distributed parameters are, hence, not changed. All parameters for the indole−water system are given in Table 1.

Finally, one of the methods used in the analysis of the result will be described. The electrostatic interaction between solute and solvent is obtained as the sum of the expectation values of the perturbation from the permanent charges of the solvent and the induced dipoles, $\hat{V}_{\text{perm}}$ and $\hat{V}_{\text{pol}}$, respectively. A multicenter multipole expansion is used to speed up evaluations of matrix elements corresponding to these operators. As a consequence, it is easy to compute the electrostatic interaction between the solvent and only a part of the indole molecule. The centers defined by atoms $C_2$ to $C_5$ and their hydrogen atoms are that part in this study, for reasons given below. We will denote this expectation value by $\langle \hat{V}_{\text{el.part}}\rangle$.

All quantum chemical calculations are done with the program package MOLCAS; QMSTAT is implemented in a local developer's version of MOLCAS.[79]

## 3. Results

**3.1. Absorption and Fluorescence in Aqueous Bulk.** In Figure 2a the solvent shift distributions for the vertical $S_0 \rightarrow L_b$ and $S_0 \rightarrow L_a$ transitions are shown. They are computed by sampling the energy difference given by eq 8,

$$\delta E = (\langle \Psi^{\text{eff}}_{\text{final}} | \hat{H}_{\text{eff}} | \Psi^{\text{eff}}_{\text{final}} \rangle - \langle \Psi^{\text{eff}}_{\text{initial}} | \hat{H}_{\text{eff}} | \Psi^{\text{eff}}_{\text{initial}} \rangle) - (\langle \Psi_{\text{final}} | \hat{H}_0 | \Psi_{\text{final}} \rangle - \langle \Psi_{\text{initial}} | \hat{H}_0 | \Psi_{\text{initial}} \rangle) \quad (8)$$

where $\Psi^{\text{eff}}_{\text{final}}$ is the effective solute wave function of the final state in the transition, $\Psi^{\text{eff}}_{\text{initial}}$ is the effective solute wave function of the initial state in the transition, and $\Psi_{\text{final}}$ and $\Psi_{\text{initial}}$ are the wave functions of the corresponding states in the gas-phase. The average shifts are 0.04 eV and −0.11 eV, respectively. Experimentally, Sun and Song find that one weakly-absorbing peak, which they assign to the $S_0 \rightarrow L_b$ transition, is very slightly blue-shifted in water as compared to nonpolar solvents.[17] Its maximum is at 4.34 eV. Hollas assigned the $S_0 \rightarrow L_b$ transition in gas-phase to a transition at 4.37 eV.[80] The $S_0 \rightarrow L_a$ transition is red-shifted, in the work by Sun and Song, as the solvent becomes more polar. The maximum for the diffuse and strongly absorbing second peak in water is determined to be 4.58 eV. The corresponding peak in the gas-phase has its maximum at 4.77 eV, according to Hollas. Comparison between our theoretical distributions and experimental spectra in solution is not straightforward; to assign the maximum in experiment is not always easy on account of overlapping or diffuse peaks, and if the intensities vary over the band, the maximum absorption does not coincide with the maximum in the density of states, which is the distribution we obtain. Because the simulation reproduces the qualitative behavior of a very slight blue-shift for the $S_0 \rightarrow L_b$ transition upon going to more polar media, we consider our result for this transition to be within the error bounds of the experiment. Judging from the values by Hollas and Sun and Song for the $S_0 \rightarrow L_a$ transition, our computed red-shift appears to be somewhat small, however. Because the experimental $S_0 \rightarrow L_a$ peak is very broad, as our distribution correctly reproduces, and has a high absorption intensity, uncertainties of the kind mentioned above in the experimental value are expected to be large. As can be seen, our distribution has a significant density at −0.19 eV (the experimental difference); hence, just a small deviation from uniform absorption intensity would take the maximum to that value.

Because QMSTAT is a state-based approach, the identity of the states are easily determined from the coefficients in eq 2. The distribution of the angle $\phi = \arctan(|c_{x3}|)/(|c_{x2}|)$ is plotted in Figure 3a, where $c_{x3}$ is the coefficient for the unperturbed $L_a$ state in the $x$th state to the effective Schrödinger equation, and $c_{x2}$ is the same for the $L_b$ state. Observe that $|c_{x2}|^2 + |c_{x3}|^2 \approx 1$ for the second and third root. The conclusion from Figure 3a is that the lowest vertically excited state is, for most configurations, well characterized as an $L_b$ state, but there are tails toward higher angles, which means that there are configurations where the pure states are more or less degenerate and are possibly in the reverse order. Together with the distributions in Figure 2a and the fact that the two states are separated by 0.3 eV in the ground state geometry in our model, the tails show that the origin of the $L_a$ peak will be below the origin of the $L_b$ peak in aqueous solution. Two-photon experiments by Rehms and Callis support this conclusion as well.[81]

To compute the shifts for the fluorescence, the identity of the lowest state must be established. In Figure 3b the mixing angle for indole in aqueous solution in the optimal $L_a$ geometry is shown, and in Figure 3c the mixing angle for indole in the optimal $L_b$ geometry is shown. In the $L_a$ geometry the states have clearly shifted, and the lowest state is a well-defined $L_a$ state. Figure 3c, on the other hand, shows that, despite a geometry optimal for the $L_b$ state, there are several configurations where the $L_a$ state is very close or even lowest in energy.

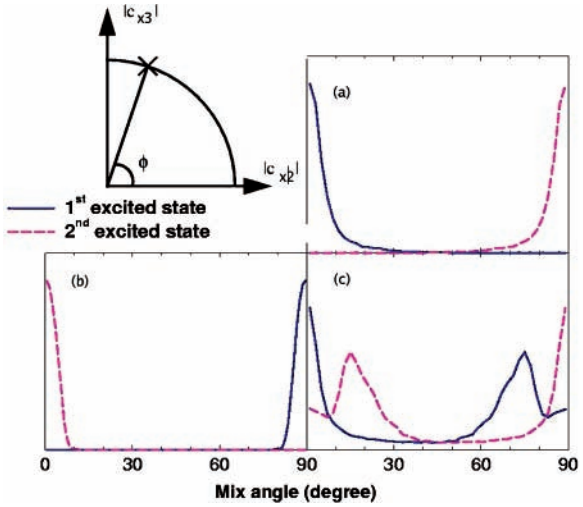


**Figure 3.** The mix angles for the first and second excited states in the (a) vertical absorption, (b) the vertical emission in the optimal $L_a$ geometry, and (c) the vertical emission in the optimal $L_b$ geometry. The mix angle is defined as the angle between the absolute values of the coefficients for the second and third basis function in eq 2 for the second and third eigenfunctions to the effective Schrödinger equation.

This means that, even if the excitation populates the $L_b$ state, the solvent perturbation will eventually put the $L_a$ state lower in energy, by which Figure 3b becomes the true description of excited indole in solution. According to the CASPT2 results by Serrano-Andrés and Roos, the energy difference in the gas-phase between the $L_a$ state in the geometry optimal for the $L_a$ state and the $L_b$ state in the geometry optimal for the $L_b$ state is 0.31 eV in favor of the $L_b$ state; the average shift of −0.58 eV for the former state (see Figure 2b), compared to ≈0.0 eV for the latter state (result not shown) also gives strong support to the interchange hypothesis. Therefore, without any prior assumptions about the fluorescing state, we conclude that the $L_a$ state is the state that in aqueous solution will be lowest in energy and thus emit light. Because the $L_a$ state does not emit in the gas-phase, it is difficult to obtain an experimental solvent shift. However, the CASPT2 calculations predict the energy difference between $L_a$ and $S_0$ to be 4.26 eV, which leads to an estimation of the fluorescence in solution to 3.68 eV. The corresponding experimental value is somewhere around 3.58 eV.

There are a number of previous theoretical studies in the literature on the absorption and emission spectra of indole in aqueous solution.[27,82−86] The $S_0 \rightarrow L_b$ transition is found by all to be only slightly shifted, though more often to the red side than to the blue side, as we find. The $S_0 \rightarrow L_a$ transition is red-shifted, but to a magnitude ranging from 0.02 to 0.19 eV. The $L_a \rightarrow S_0$ transition from the optimal $L_a$ geometry is found to be red-shifted in all previous studies, although the reported energies go from 0.26 to 0.81 eV. The different studies use various quantum chemical methods and solvent representations; it is thus difficult, if not impossible, to clarify the causes to the very different results. We make two observations, however. Muino and Callis obtain the large shift 0.81 eV from their semiempirical/molecular mechanics study of the fluorescence. In their model, the shift derives completely from the electrostatic interaction. A clue to their large shift, as compared with our result, is found in the dipole of the solvated $L_a$ state. Muino and Callis report an average value of 13.03 D, which as compared with our value of 9.6 D is quite large. The $L_a$ state is thus expected to be more stabilized by the solvent in the study of Muino and Callis than in our study; hence, the shifts are expected to qualitatively differ in the way they do. The second

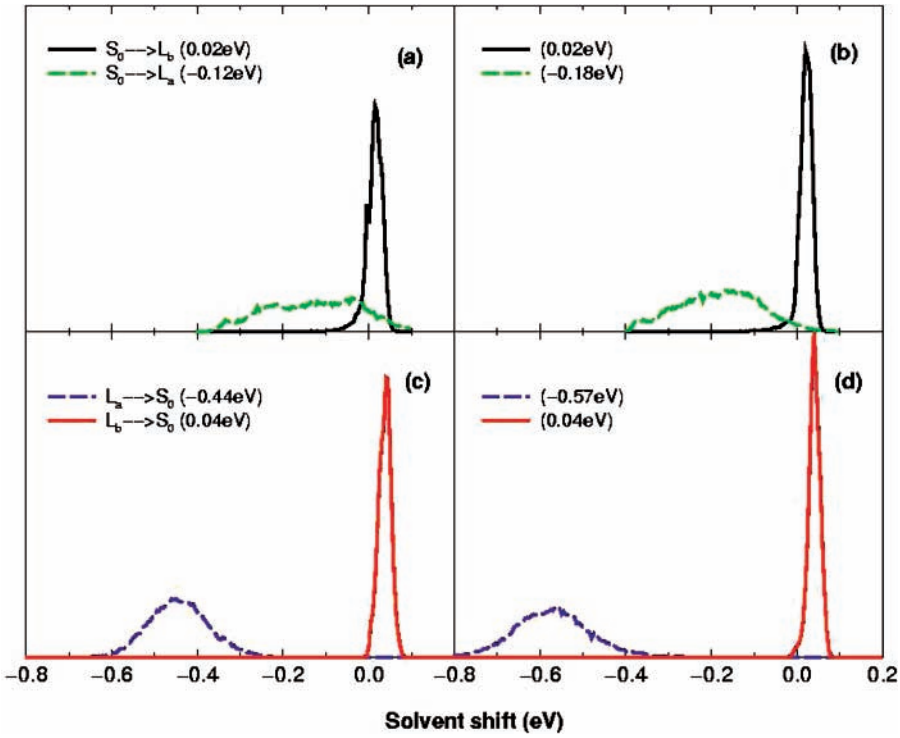


**Figure 4.** The solvent shift distribution for (a) F-initialized absorption, (b) W-initialized absorption, (c) F-initialized fluorescence for the $L_a$ geometry and (d) W-initialized fluorescence for the $L_a$ geometry.

observation concerns the small shift for the same transition reported by Serrano-Andrés and Roos (0.26 eV). Their quantum chemical method is very similar to ours, but they use a continuum description of the solvent. The authors suggest that their small shift derives from their neglect of the contribution to the shift from the dispersion interaction. We do not include this contribution either, hence this interpretation by Serrano-Andrés and Roos seems to be, at least, incomplete. We suggest instead that some combination of (i) a poor description of hydrogen bonding between water and indole, (ii) a too large cavity, as well as (iii) a complete disregard of fluctuations in the electric field from the solvent in continuum models better explains the small shift. As will be shown later, the former property can have a significant effect on the studied transition, and the third deficiency of continuum descriptions, or solvent mean-field theories, has been discussed elsewhere.[87−89] This does not rule out that the dispersion interactions can contribute with an additional red-shift or that further relaxations of the geometry of indole in solution also does so. However, most of the discrepancy of the shift in the study by Serrano-Andrés and Roos can be explained by the three limitations of their continuum model listed above.

**3.2. Absorption and Fluorescence at a Nonpolar/Polar Interface.** In Figure 4 are four solvent shift distributions shown for absorption and fluorescence at the air/water interface. Two types of indole-interface structures have been studied through "flat"-initialized (F-initialized) and "wedge"-initialized (W-initialized) simulations. The F-initialized simulations have indole laying more-or-less horizontally on the surface, although in most configurations a single water molecule is hydrogen-bonded to the pyrrole part. The W-initialized simulations have indole cutting into the surface with its pyrrole part, thus keeping the benzene part out of the water. Snap-shots of typical structures are shown in Figure 5. No constraints have been applied to the simulations to maintain a certain relative orientation between solute and interface. Although such constraints could be used to study the dependence of the shifts on orientations relative to

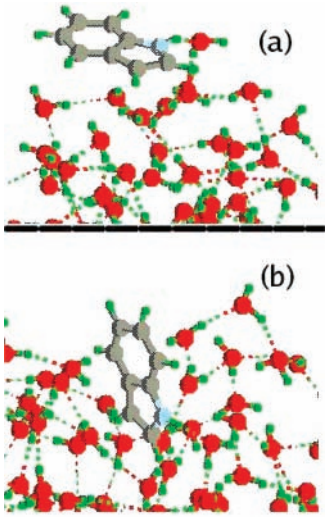


**Figure 5.** Snap-shots from the (a) F-initialized and the (b) W-initialized simulations of indole at the air−water interface. In the former case the indole molecule lays roughly horizontally on the surface, whereas in the latter case indole cuts into the surface with the pyrrole part pointing inward and the benzene part outward.

the interface in detail, they are hard to define because the interface is neither continuous nor monotone in shape. As a consequence, the constraints become ambiguous, and there is a risk that the system responds to them in ways not intended. For example, the optimal orientation between indole and its immediate air/water surface, in the case of no constraint, could be obtained despite a constraint added, because the system could be perturbed such that the ambiguously defined orientation still fulfills the constraint. On the other hand, because the indole molecule is not rotated in the global coordinate system of the simulation, it is a lengthy process for the system to go from a F-type configuration to a W-type configuration; the entire water drop has to translate 90 degrees relative a fixed indole molecule. This leads to the conclusion that the differently initialized

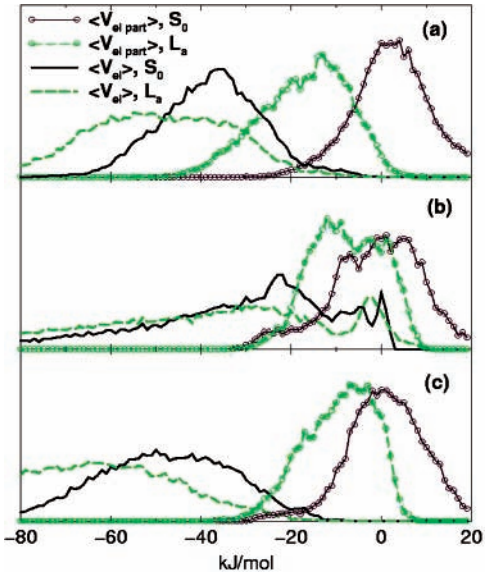


**Figure 6.** Distributions of solute−solvent electrostatic interaction and partial solute−solvent electrostatic interaction for (a) the bulk simulation of the ground state of indole, (b) the F-initialized simulation of the same state and (c) the W-initialized simulation.

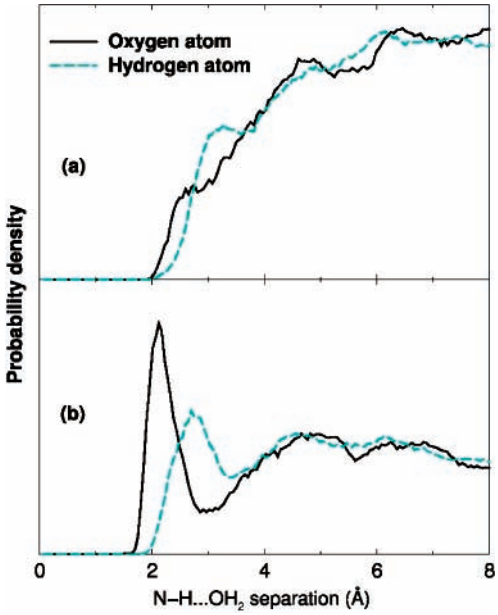


**Figure 7.** Radial probability density distribution for (a) bulk simulations and (b) W-initialized simulations of the ground state. Observe that the distributions are not exactly comparable, hence the vertical axis is given in arbitrary units because quantitative comparisons only are possible within each distribution, not between.

simulations can be considered to be partially in equilibrium, because the other degrees of freedom are optimized more easily, whereas the relative orientation to the surface is qualitatively the same. The exact nature of the orientation of indole at an air/water interface is thus not resolved by the present study. This is not our goal, though; instead, two special orientations are studied without the enforcing of ambiguous constraints.

Figure 4, panels a and b, shows the distributions for the vertical transitions $S_0 \rightarrow L_a$ and $S_0 \rightarrow L_b$. In addition to being almost unaffected by the transition from bulk to surface, the $L_b$ state is not the fluorescing state at the surface either, as will be shown; hence, we limit our analysis to the $S_0 \rightarrow L_a$ transition. We find the average shift at the interface for this transition to be not smaller but larger than in bulk solution; in the W-initialized simulation this is significantly so. To analyze this result, the distribution of the electrostatic interaction between solute and solvent $\langle V_{el} \rangle$ and of the partial electrostatic interaction between solvent and the far side of the benzene part $\langle V_{el.part} \rangle$, as described in the end of the Method and Computational Protocol section, are plotted; see Figure 6. In all simulations the partial electrostatic interaction with the benzene part becomes more attractive in the $L_a$ state as compared to $S_0$. Because additional charge accumulates in the benzene part in the $L_a$ state, a modification is expected, but because the transition is vertical, it is not obvious that it will be to the attractive side. Furthermore, the difference in $\langle V_{el.part} \rangle$ between $S_0$ and $L_a$ is smaller at the surface than in the bulk. It is the expected result when the dielectric medium at the benzene-side of indole disappears at the surface. We call this a dielectric depletion effect. Alone, this effect leads to a smaller shift at the surface. The total electrostatic interaction, however, increases at the surface for the W-initialized simulation, as seen from the $\langle V_{el} \rangle$ distributions. Therefore, by exclusion, the solvent interaction with the pyrrole part of indole has to increase at the surface. This has to be because of some interface-specific effect, that is, a different kind of indole−water interaction appears in the presence of the surface. Because the effective interactions at the air/water interface is a coupled energy and entropy balance between water−indole, water−water, indole−air, and water−air interactions, any specific effects the nonpolar air-phase has on either solute or solvent can induce changes beyond the given interaction pair. We suggest an explanation of the interface-specific effect of the indole absorption spectra based on previous results on hydrogen bonding at nonpolar interfaces.[38,39,43,90−94] It has been shown, first by simulations and later by experiments, that water at a nonpolar interface forms more and stronger hydrogen bonds per nearest neighbor. Because the pyrrole part of indole has the ability to form a hydrogen bond with water, the presence of the surface could induce the adjacent water to form stronger hydrogen bonds than in the aqueous bulk. In the bulk there is an abundance of other water molecules to form strong hydrogen bonds with; hence, water nearby indole under such conditions is not expected to form, from an energetic point of view, optimal hydrogen bonds with indole. In contrast, at the surface, where the bonding options are reduced, the adjacent water molecules will orient themselves relative to indole such that the hydrogen bonding to it increases. This will stabilize both the ground and the $L_a$ state, but it will affect the latter state the most because it forms stronger hydrogen bonds with water, according to our supermolecular calculations (recall that the excitation is vertical, hence the solvent structure is optimal to the ground state). In Figure 7 the radial probability density distribution around the hydrogen atom bonded to the nitrogen atom is shown for bulk and W-initialized simulations of the ground state. As seen, there is a weak preference for the oxygen atom of water to be closest to the hydrogen atom of the pyrrole part in the bulk, whereas at the surface the preference is much more pronounced. It should be noted that the two radial distributions are not exactly comparable because the isotropy is broken at the surface, and less solvent is present at longer distances than in bulk. Still, the steep growth of the distribution function at the surface at short distances can not only be justified by the broken isotropy, because at these short distances the surface has not yet been reached for the W-initialized simulations. We therefore propose that the increased strength of the hydrogen bonds between indole and water, induced by the presence of the nonpolar air-surface, is the cause of the specific surface effect and, hence, the increased shift of the $S_0 \rightarrow L_a$ transition compared to the aqueous bulk.

A short comment in Figure 7a is justified before the surface simulation is further analyzed. This figure suggests that only weak hydrogen bonds are formed between indole and water, despite that the pair-potential energy has a minimum of similar depth as the water−water potential energy (result not shown, but see refs 71 and 95). As already noted above, this hydrogen bond in aqueous bulk is not expected to take its maximal strength. Some care should also be exercised when radial distributions are analyzed for a nonspherical object such as indole where angular features also are of significance; as the separation takes larger values, regions from which water is excluded at shorter separations becomes available; hence, the radial distribution is expected to increase in the way it does, therefore making the initial peak seem smaller. We conclude, therefore, that the radial distribution in Figure 7a does not have to contradict the results for the indole−water pair-potential.

The distribution for the F-initialized simulation in Figure 6b departs from the other two simulations. A closer analysis of the simulation shows that it consists of roughly two types of configurations: one type with indole laying on the surface, which gives relatively small electrostatic interaction energies and shifts; and another type with indole more surrounded by solvent, with larger interaction energies and shifts. It means that the partial equilibrium, as discussed above, is not perfectly maintained in the F-initialized simulation. This does not rule out that F-type configurations appear at an air/water interface, only that it is not the only configuration. The hydrogen bonding also is important in the pure F-type configurations, but the small interaction in these configurations shows that only hydrogen bonding is not enough to bring about interactions and shifts of the same magnitude as found in the W-initialized simulations.

An analysis of the wave function for the first and second excited-state in both ground and excited-state at the surface support the same conclusions as in the bulk. That is, in the ground state the vertically excited states have the $L_b$ state first, followed at higher energies by the $L_a$ state; in the $L_a$ geometry, the first excited-state is a well-defined $L_a$ state, whereas in the $L_b$ geometry, significant mixing can occur, and thus the $L_a$ state is predicted to be the fluorescing state also at the interface. For this reason, we limit the detailed analysis of the fluorescence at the interface to the $L_a$ geometry.

The distributions of $\langle V_{el}\rangle$ and $\langle V_{el.part}\rangle$ for the fluorescence in the $L_a$ geometry show the same qualitative features as in the absorption, but the magnitudes are different; see Figure 8. The decrease in the magnitude of $\langle V_{el.part}\rangle$ in leaving the bulk and going to the surface shows that the dielectric depletion effect works here as well. The slight increase in the magnitude of $\langle V_{el}\rangle$, despite the dielectric depletion effect, further shows that an interface-specific effect also operates, which, as before, we assign to stronger hydrogen bonding at the surface. The quite different magnitude of the electrostatic interaction between the absorption and fluorescence comes from the orientational and packing relaxation of the solvent around indole in its very polar excited state. The $L_a$ state becomes very stabilized by the reaction field from the solvent, but the vertically de-excited ground state also is more stabilized. However, the relative numbers differ more, thus large solvent shifts are obtained for the fluorescence in the bulk (Figure 2b) and at the surface (Figure 4, panels c and d). The specific surface effect is not strong enough in the fluorescence to make the shifts larger at the surface than in the bulk. The greater importance of the ordinary dielectric effect and the already in bulk strong hydrogen bonds for the $L_a$ state are the cause of this.

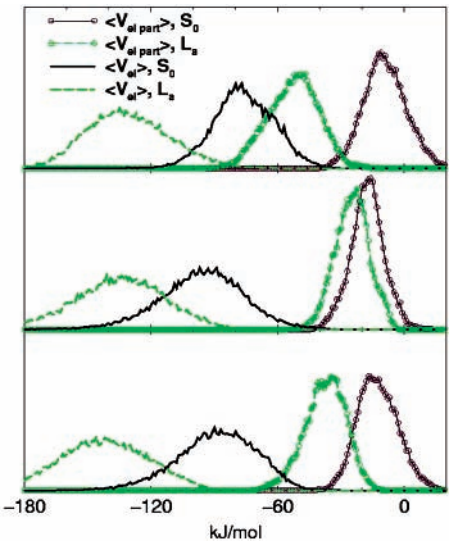


**Figure 8.** Distributions of solute−solvent electrostatic interaction and partial solute−solvent electrostatic interaction for (a) the bulk simulation of the first excited-state of indole in the $L_a$ geometry, (b) the F-initialized simulation of the same state, and (c) the W-initialized simulation.

## 4. Conclusions

With an ab initio quantum chemical method coupled to a discrete and polarizable solvent, we have computed the solvent shifts of the absorption and fluorescence of indole in aqueous solution. The results agree well with experiments. We have made no assumptions about the nature of the fluorescing state of indole or parametrizations based on experiment, and we have only used the intermolecular interaction between indole and water, obtained from ab initio quantum chemical calculations, as input into the model. We observe a $L_a-L_b$ state interchange, which has been used to explain the characteristic fluorescence of indole and tryptophan in a polar medium. Therefore, our calculations provide strong support to the interchange mechanism.

To shed light on the photophysics of the amino acid tryptophan, which has indole as its chromophore, in a protein environment, we have modeled the photophysics at the air/water interface instead of modeling the complete protein, a task fraught with difficulties and possible model artifacts. Two important conclusions about indole at a polar/nonpolar interface are found. First, being at the interface does not necessarily lead to a significant reduction in the solvent shift as compared to being in the bulk. We identify two counteracting effects to explain this. On one hand is the dielectric depletion effect, which reduces the shift when less polar medium is able to respond to the dipole of indole. On the other hand is the interface-specific effect, which involves stronger hydrogen bonding at the surface or interface that especially favors a greater stabilization of the excited-state and thus leads to a larger magnitude of the red-shift. Second, the orientation of the chromophore relative to the interface is of importance, because the dielectric depletion and interface-specific effects are of different importance in different orientations.

These qualitative conclusions are likely to be transferable to protein environments and are not only of interest for studies of the air/water interface. If a tryptophan amino acid in a protein is located at a protein/water interface, then the recorded shift can, on account of the surface-specific effect, depend on subtle features such as how water interacts with the protein residues nearby the tryptophan amino acid. Further, the orientation of tryptophan relative to the nearby waters will also be of importance. For differently folded states of a protein, not only

can the degree of exposure of the amino acid to the polar medium be different but also these two additional effects. There is, of course, also an additional effect from the perturbation on the chromophore by polar groups on nearby amino acids, which has not been considered here. The many different contributions to the total shift of the fluorescence of tryptophan precludes detailed relations between structure and magnitude of shift to be formulated.

A general conclusion from this study is that an interface can give rise to subtle effects in the spectrum of chromophores, especially if one of the phases is a protic solvent. The surface affinity of the chromophore, its orientation at the interface, its hydrogen-bonding capacity in the relevant states, and the effective influence the interface has on the solvent−solvent and solvent−solute interaction are all aspects that are of relevance for the spectrum, apart from the usual properties. Further knowledge of these different features will improve our understanding of how a chromophore, or a chemical process in general, behave in heterogeneous and interfacial environments.

**Acknowledgment.** Financial support from the Swedish Research Council within the Linné-project Organizing Molecular Matter is acknowledged. Computer time at Lunarc, Center for Scientific and Technical Computing, Lund University is acknowledged.

## References and Notes

(1) Witt, O. N. *Ber. Dtsch Chem. Ges.* **1876**, *9*, 522−527.
(2) Beer, J. J. *Isis* **1958**, *49*, 123−131.
(3) Ihde, A. J. *The Development of Modern Chemistry*; Dover Publications: New York, 1964.
(4) Meyer-Thurow, G. *Isis* **1982**, *73*, 363−381.
(5) Kasha, M. *Discuss. Faraday Soc.* **1950**, *9*, 14−19.
(6) McConnell, H. *J. Chem. Phys.* **1952**, *20*, 700−704.
(7) Reichardt, C. *Chem. Rev.* **1994**, *94*, 2319−2358.
(8) Reichardt, C. *Solvents and Solvent Effects in Organic Chemistry*, 3rd ed; Wiley-VCH: Weinheim, 2003.
(9) Beechem, J. M.; Brand, L. *Annu. Rev. Biochem.* **1985**, *54*, 43−71.
(10) Valeur, B. *Molecular Fluorescence, Principles and Applications;* Wiley-VCH: Weinheim, 2001.
(11) Jameson, D. M.; Croney, J. C.; Moens, P. D. J. *Methods Enzymol.* **2003**, *360*, 1−43.
(12) Royer, C. A. *Chem. Rev.* **2006**, *106*, 1769−1784.
(13) Teale, F. W. J.; Weber, G. *Biochem. J.* **1957**, *65*, 476−482.
(14) van Duuren, B. L. *J. Org. Chem.* **1961**, *26*, 2954−2960.
(15) van Duuren, B. L. *Chem. Rev.* **1963**, *63*, 325−354.
(16) Mataga, N.; Torihashi, Y.; Ezumi, K. *Theor. Chim. Acta* **1964**, *2*, 158−167.
(17) Sun, M.; Song, P.-S. *Photochem. Photobiol.* **1977**, *25*, 3−9.
(18) Creed, D. *Photochem. Photobiol.* **1984**, *39*, 537−562.
(19) Sharma, N.; Jain, S. K.; Rastogi, R. C. *Spectrochim. Acta A* **2007**, *66*, 171−176.
(20) Platt, J. R. *J. Chem. Phys.* **1949**, *17*, 489−495.
(21) Weber, G. *Biochem. J.* **1960**, *75*, 335−345.
(22) Walker, M. S.; Bednar, T. W.; Lumry, R. *J. Chem. Phys.* **1967**, *47*, 1020−1028.
(23) Lami, H.; Glasser, N. *J. Chem. Phys.* **1986**, *84*, 597−604.
(24) Vekshin, N.; Vincent, M.; Gallay, J. *Chem. Phys. Lett.* **1992**, *199*, 459−464.
(25) Carney, J. R.; Zwier, T. S. *J. Phys. Chem. A* **1999**, *103*, 9943−9957.
(26) Chang, C. T.; Wu, C. Y.; Muirhead, A. R.; Lombardi, J. R. *Photochem. Photobiol.* **1974**, *19*, 347−351.
(27) Serrano-Andrés, L.; Roos, B. O. *J. Am. Chem. Soc.* **1996**, *118*, 185−195.
(28) Lombardi, J. R. *J. Phys. Chem. A* **1999**, *103*, 6335−6338.
(29) Vivian, J. T.; Callis, P. R. *Biophys. J.* **2001**, *80*, 2093−2109.
(30) Somers, K. R. F.; Ceulemans, A. *J. Phys. Chem. A* **2004**, *108*, 7577−7583.
(31) Jalviste, E.; Ohta, N. *J. Chem. Phys.* **2004**, *121*, 4730−4739.
(32) Kang, C.; Korter, T. M.; Pratt, D. W. *J. Chem. Phys.* **2005**, *122*, 174301.
(33) Kang, C.; Pratt, D. W. *Int. Rev. Phys. Chem.* **2005**, *24*, 1−36.
(34) Andrews, L. J.; Forster, L. S. *Biochemistry* **1972**, *11*, 1875−1879.
(35) Snoek, L. C.; Kroemer, R. T.; Hockridge, M. R.; Simons, J. P. *Phys. Chem. Chem. Phys.* **2001**, *3*, 1819−1826.
(36) Koenig, S.; Müller, L.; Smith, D. K. *Chem.—Eur. J.* **2001**, *7*, 979−986.
(37) Rogers, D. M.; Besley, N. A.; O'Shea, P.; Hirst, J. D. *J. Phys. Chem. B* **2005**, *109*, 23061−23069.
(38) Benjamin, I. *Chem. Rev.* **1996**, *96*, 1449−1475.
(39) Richmond, G. L. *Chem. Rev.* **2001**, *102*, 2693−2724.
(40) Mmereki, B. T.; Donaldson, D. J. *Phys. Chem. Chem. Phys.* **2002**, *4*, 4186−4191.
(41) Mmereki, B. T.; Chaudhuri, S. R.; Donaldson, D. J. *J. Phys. Chem. A* **2003**, *107*, 2264−2269.
(42) Steel, W. H.; Walker, R. A. *J. Am. Chem. Soc.* **2003**, *125*, 1132−1133.
(43) Benjamin, I. *Chem. Rev.* **2006**, *106*, 1212−1233.
(44) Sobolewski, A. L.; Domcke, W. *Chem. Phys. Lett.* **1999**, *315*, 293−298.
(45) Dian, B. C.; Longarte, A.; Zwier, T. S. *J. Chem. Phys.* **2003**, *118*, 2696−2706.
(46) Nix, M. G. D.; Devine, A. L.; Cronin, B.; Ashfold, M. N. R. *Phys. Chem. Chem. Phys.* **2006**, *8*, 2610−2618.
(47) Dedonder-Lardeux, C.; Jouvet, C.; Perun, S.; Sobolewski, A. L. *Phys. Chem. Chem. Phys.* **2003**, *5*, 5118−5126.
(48) Bayliss, N. S.; McRae, E. G. *J. Phys. Chem.* **1954**, *58*, 1002−1006.
(49) Öhrn, A.; Karlström, G. *Mol. Phys.* **2006**, *104*, 3087−3099.
(50) Öhrn, A.; Aquilante, F. *Phys. Chem. Chem. Phys.* **2007**, *9*, 470−480.
(51) Wallqvist, A.; Ahlström, P.; Karlström, G. *J. Phys. Chem.* **1990**, *94*, 1649−1656.
(52) Friedman, H. L. *Mol. Phys.* **1975**, *29*, 1533−139.
(53) Wallqvist, A. *Mol. Sim.* **1993**, *10*, 13−17.
(54) Metropolis, N.; Rusenbluth, A. W.; Rusenbluth, M. N.; Teller, A.; Teller, E. *J. Chem. Phys.* **1953**, *21*, 1087−1092.
(55) Öhrn, A.; Karlström, G. *Theor. Chem. Acc.* **2007**, *117*, 441−449.
(56) Moriarty, N. W.; Karlström, G. *J. Phys. Chem.* **1996**, *100*, 17791−17796.
(57) Roos, B. O.; Taylor, P. R.; Siegbahn, P. E. M. *Chem. Phys.* **1980**, *48*, 157−173.
(58) Roos, B. O. *Adv. Chem. Phys.* **1987**, *69*, 399−445.
(59) Roos, B. O.; Andersson, K.; Fülscher, M. P. *Chem. Phys. Lett.* **1992**, *192*, 5−13.
(60) Pierloot, K.; Dumez, B.; Widmark, P.-O.; Roos, B. O. *Theor. Chim. Acta* **1995**, *90*, 87−114.
(61) Stålring, J.; Bernhardsson, A.; Lindh, R. *Mol. Phys.* **2001**, *99*, 103−114.
(62) Malmqvist, P. Å. *Int. J. Quant. Chem.* **1986**, *30*, 479−494.
(63) Malmqvist, P. Å.; Roos, B. O. *Chem. Phys. Lett.* **1989**, *155*, 189−194.
(64) Andersson, K.; Malmqvist, P.-Å.; Roos, B. O.; Sadlej, A. J.; Wolinski, K. *J. Phys. Chem.* **1990**, *94*, 5483−5488.
(65) Andersson, K.; Malmqvist, P.-Å.; Roos., B. O. *J. Chem. Phys.* **1992**, *96*, 1218.
(66) Roos, B. O.; Andersson, K.; Fülscher, M. P.; Malmqvist, P.-Å.; Serrano-Andrés, L.; Pierloot, K.; Merchán, M. *Adv. Chem. Phys.* **1996**, *93*, 219−331.
(67) Serrano-Andrés, L.; Merchán, M. *J. Mol. Struct.* **2005**, *729*, 99−108.
(68) Parac, M.; Grimme, S. *J. Phys. Chem. A* **2002**, *106*, 6844−6850.
(69) Boys, S. F.; Bernardi, F. *Mol. Phys.* **1970**, *19*, 553−566.
(70) Mons, M.; Dimicoli, I.; Tardivel, B.; Piuzzi, F.; Brenner, V.; Millié, P. *J. Phys. Chem. A* **1999**, *103*, 9958−9965.
(71) van Mourik, T.; Price, S. L.; Clary, D. C. *Chem. Phys. Lett.* **2000**, *331*, 253−261.
(72) Zhang, R. B.; Somers, K. R. F.; Kryachko, E. S.; Nguyen, M. T.; Zeegers-Huyskens, T.; Ceulemans, A. *J. Phys. Chem. A* **2005**, *109*, 8028−8034.
(73) Tang, K. T.; Toennies, J. P. *J. Chem. Phys.* **1984**, *80*, 3726−3741.
(74) Brdarski, S.; Karlström, G. *J. Phys. Chem. A* **1998**, *102*, 8182−8192.
(75) Becke, A. D.; Johnson, E. R. *J. Chem. Phys.* **2005**, *122*, 154104.
(76) Johnson, E. R.; Becke, A. D. *J. Chem. Phys.* **2005**, *123*, 024101.
(77) Lindh, R.; Malmqvist, P.-Å.; Gagliardi, L. *Theor. Chem. Acc.* **2001**, *106*, 178−187.
(78) Gagliardi, L.; Lindh, R.; Karlström, G. *J. Chem. Phys.* **2004**, *121*, 4494−4500.
(79) Karlström, G.; Lindh, R.; Malmqvist, P.-Å.; Roos, B. O.; Ryde, U.; Veryazov, V.; Widmark, P.-O.; Cossi, M.; Schimmelpfennig, B.; Neogrady, P.; Seijo, L. *Comp. Mater. Sci.* **2003**, *28*, 222−239.
(80) Hollas, J. M. *Spectrochim. Acta* **1963**, *19*, 753−767.
(81) Rehms, A. A.; Callis, P. R. *Chem. Phys. Lett.* **1993**, *208*, 276−282.

(82) Ilich, P.; Haydock, C.; Prendergast, F. G. *Chem. Phys. Lett.* **1989**, *158*, 129−134.
(83) Chabalowski, C. F.; Garmer, D. R.; Jensen, J. O.; Krauss, M. *J. Phys. Chem.* **1993**, *97*, 4608−4613.
(84) Muino, P. L.; Callis, P. R. *J. Chem. Phys.* **1994**, *100*, 4093−4109.
(85) Serrano-Andrés, L.; Fülscher, M. P.; Karlström, G. *Int. J. Quant. Chem.* **1997**, *65*, 167−181.
(86) Rogers, D. M.; Hirst, J. D. *J. Phys. Chem. A* **2003**, *107*, 11191−11200.
(87) Baur, M. E.; Nicol, M. *J. Chem. Phys.* **1966**, *44*, 3337−3343.
(88) Karlström, G.; Halle, B. *J. Chem. Phys.* **1993**, *99*, 8056−8062.
(89) Öhrn, A.; Karlström, G. *J. Chem. Theory Comput.* in press, [Online] DOI: ct700022b.
(90) Lee, C. Y.; McCammon, J. A.; Rossky, P. J. *J. Chem. Phys.* **1984**, *80*, 4448−4455.
(91) Linse, P. *J. Chem. Phys.* **1987**, *86*, 4177−4187.
(92) Wallqvist, A. *Chem. Phys. Lett.* **1990**, *165*, 437−442.
(93) Du, Q.; Superfine, R.; Freysz, E.; Shen, Y. R. *Phys. Rev. Lett.* **1993**, *70*, 2313−2316.
(94) Liu, P.; Harder, E.; Berne, B. J. *J. Phys. Chem. B* **2005**, *109*, 2949−2955.
(95) Schütz, M.; Brdarski, S.; Widmark, P.-O.; Lindh, R.; Karlström, G. *J. Chem. Phys.* **1997**, *197*, 4597−4605.